Study of equilibrium carrier transfer in $LaAlO_3/SrTiO_3$ from an epitaxial $La_{1-x}Sr_xMnO_3$ ferromagnetic layer

Journal of Physics Communications

PAPER

Study of equilibrium carrier transfer in LaAlO₃/SrTiO₃ from an epitaxial La$_{1-x}$Sr$_x$MnO₃ ferromagnetic layer

F Telesio[1,7], R Moroni[1], I Pallecchi[1] , D Marré[1], G Vinai[2] , G Panaccione[2], P Torelli[2], S Rusponi[3], C Piamonteze[4], E di Gennaro[5], A Khare[5,8], F Miletto Granozio[5] and A Filippetti[6]

1   CNR-SPIN Genova and Università di Genova, Dipartimento di Fisica, via Dodecaneso 33, I-16146 Genova, Italy
2   CNR-IOM, Laboratorio TASC in Area Science Park, S.S. 14 km 163.5, Basovizza, I-34149 Trieste, Italy
3   IPHYS-Institute of Physics, EPFL École Polytechnique Fédérale de Lausanne, Station 3, CH-1015 Lausanne, Switzerland
4   Swiss Light Source, Paul Scherrer Institute, 5232 Villigen-PSI, Switzerland
5   CNR-SPIN Napoli and Dipartimento di Fisica, Università di Napoli 'Federico II,' I-80126 Napoli, Italy
6   Dipartimento di Fisica Università di Cagliari and CNR-IOM Cagliari, Cittadella Universitaria, Monserrato (CA) I-09042-I, Italy
7   Present address: NEST, Istituto Nanoscienze-CNR and Scuola Normale Superiore, Piazza S. Silvestro 12, I-56127 Pisa, Italy.
8   Present address: Department of Physics, Indian Institute of Science, Education and Research, Bhopal—462 066, (India).

E-mail: Ilaria.pallecchi@spin.cnr.it

Abstract

Using x-ray magnetic circular dichroism and ab-initio calculations, we explore the La$_{1-x}$Sr$_x$MnO₃/LaAlO₃/SrTiO₃ (001) heterostructure as a mean to induce transfer of spin polarized carriers from ferromagnetic La$_{1-x}$Sr$_x$MnO₃ layer into the 2DEG (two-dimensional electron gas) at the LaAlO₃/SrTiO₃ interface. By out-of-plane transport measurements, the tunneling across the LaAlO₃ barrier is also analyzed. Our results suggest small or vanishing spin-polarization for the 2DEG: magnetic dichroism does not reveal a neat signal on Ti atoms, while calculations predict, for the pristine stoichiometric interface, a small spin-resolved mobile charge of 2.5×10^{13} cm^{-2} corresponding to a magnetic moment of 0.038 μ_B per Ti atom, tightly confined within the single SrTiO₃ layer adjacent to LaAlO₃. Such a small magnetization is hard to be detected experimentally and perhaps not robust enough to survive to structural disorder, native doping, or La$_{1-x}$Sr$_x$MnO₃ dead-layer effects. Our analysis suggests that, while some spin-diffusion cannot be completely ruled out, the use of ferromagnetic La$_{1-x}$Sr$_x$MnO₃ epilayers grown on-top of LaAlO₃/SrTiO₃ is not effective enough to induce robust spin-transport properties in the 2DEG. The examined heterostructure is nevertheless an excellent test-case to understand some fundamental aspects of the spin-polarized charge transfer in 2D wells.

1. Introduction

The discovery of a two-dimensional electron gas (2DEG) at the interface between high bandgap perovskite oxides LaAlO₃ (LAO) and SrTiO₃ (STO) [1] has renewed the interest in exploring the potential of oxide electronics, with the exciting perspective to fabricate novel devices [2, 3] which integrate in a single crystalline heterostructure multiple functionalities such as high-T_c superconductivity, ferroelectricity, and ferromagnetism. It is demonstrated that both charge and spin of the conduction electrons in LAO/STO offer the possibility to manipulate and store digital information. Indeed, a strong Rashba spin—orbit coupling tunable by an applied gate voltage is observed [4, 5], suggesting that transport of spin polarized carriers can be controlled by external parameters. Nevertheless, while charge transport in LAO/STO has been widely explored, spin transport remained an uncharted topic until very recently, at least on the experimental ground. Ferromagnetic puddles may be induced in LAO/STO by oxygen vacancies [6], yet stoichiometric LAO/STO is thought to be nonmagnetic. Attempts of delta doping with magnetic epilayers inserted between LAO and STO to induce a spin-polarized electron gas were carried out, but in most cases the charge at the interlayer ended up to be localized [7, 8]. Remarkable exceptions are represented by the insertion of thin magnetic epitaxial EuTiO₃ (ETO)

and $La_{7/8}Sr_{1/8}MnO_3$ interlayers at the LAO/STO interface. Specifically, a ETO layer at the interface, resulted in a conducting and ferromagnetic (FM) LAO/ETO/STO heterostructure [9], with net spin-polarized charge carriers induced in the 2DEG [10]. Similarly, a interfacial manganite layer with controlled interdiffusion gave rise to gate tunable anomalous Hall effect and enhanced mobility in the 2DEG [11]. In [12], the role of charge polarity of SrO and LaO atomic layers in the charge transfer across a sandwiched MnO_2 layer was demonstrated, resulting in a 2D ferromagnetic metallic state in the case that MnO_2 is stacked between two LaO layers.

Alternatively, injection and/or diffusion of spin-polarized charge in LAO/STO could be achieved using FM electrodes deposited on top; this is a promising route since the *in situ* deposition of FM overlayers better preserves the interface sharpness as compared to the inclusion of FM interlayers. In FM/LAO/STO heterostructures, significant inverse Edelstein effect is measured by spin pumping using ferromagnetic resonance [13, 14] and large charge-to-spin conversion is detected by spin torque ferromagnetic resonance [15]. Evidences of long range (several nm) magnetic interactions in the $La_{0.67}Sr_{0.33}MnO_3/LaAlO_3/SrTiO_3$ heterostructure, affecting both the magnetic properties of $La_{0.67}Sr_{0.33}MnO_3$ and the electric transport in the 2DEG at the $LaAlO_3/SrTiO_3$ interface are reported in [16], where the underlying mechanism is discussed in terms of orbital correlations across the polar insulating barrier. An induced spin polarization in a 2DEG was previously observed in various FM/2DEG systems like MnAs/GaAs and Fe/GaAs [17]. However, there is no clear evidence, so far, that this route to 2DEG magnetization can work for LAO/STO as well. In literature only a couple of cases report electric spin transfer from on-top magnetic electrodes into LAO/STO [18, 19]. In particular, reference [18] reports transfer from FM Co electrodes with surprisingly long in-plane spin diffusion length of $d_{spin} \sim 1$ μm in the 2DEG, as estimated by Hanle effect, which is much larger than the estimate derived from the analysis of weak localization magnetoresistance [4], but consistent with estimates extracted from spin Hall effect in a non-local geometry [5]. In the same reference [18], the authors suggest that interface defects may play a role in amplifying the spin accumulation signal through a resonant tunneling mechanism. Very recently, spin-polarized carrier injection in LAO/STO generated by spin pumping from a permalloy electrode and detected by inverse spin-Hall effect in Pt and Ta electrodes [20] indicated an in-plane spin diffusion lengths in the range of 200–350 nm at room temperature, corresponding to spin lifetimes of ∼2–6 ns. Predictions based on effective spin—orbit Hamiltonians for non-magnetic materials [21] suggest that long spin lifetimes in LAO/STO can be actually achieved. On the other hand, x-ray magnetic circular dichroism measurements on Co/LAO/STO heterostructures show small (∼10^{-2} μ_B per Ti atom) spin polarization of diffused carriers in LAO/STO capped with a 2.5 nm-thick Cobalt film [22]. Consistently, *ab-initio* calculations [23] show that a one unit cell thick FM Ti overlayer injects ∼0.04 μ_B per atom in LAO/STO, while, Fe, Co, and Pt, are unable to inject any significant spin polarization in the 2DEG even for a LAO barrier as thin as 2 unit cells.

These contrasting evidences call for further scrutiny and investigation of possible spin polarization by proximity effect or spin injection and diffusion in FM/LAO/STO heterostructures. A univocal determination of the spin polarization and spin-transport capabilities for LAO/STO is made difficult by the many factors which can severely affect spin transport at both extrinsic and intrinsic level, related to growth and processing. Clearly, the use of extremely clean and flawless heterostructures is crucial, since, at the most fundamental level, transfer of spin-polarized carriers is governed by band alignment across the heterostructure. *Ab-initio* calculations are ideally suited to study the electronic properties of the heterostructures, provided that advanced methodologies are used, capable to overcome the typical inaccuracies in the treatment of oxide systems proper of standard *ab-initio* approaches.

In this work, we use a combination of x-ray absorption spectroscopy (XAS) and magnetic circular dichroism (XMCD), current-voltage measurements, and beyond-standard variational pseudo self-interaction correction density functional (VPSIC) calculations to investigate the actual possibility to induce spin transfer from a FM overlayer in LAO/STO under equilibrium conditions. To this aim, we consider a significant test case, namely the epitaxial $La_{0.67}Sr_{0.33}MnO_3$(LSMO)/LAO/STO heterostructure grown along the [001] direction. The LSMO overlayer, a half-metallic ferromagnet with 100% spin-polarization at the Fermi level, represents in principle an optimal candidate. Nevertheless, measurements and calculations coherently indicate absence of sizeable spin transfer across the interface. Specifically, XMCD does not show any sizable signal above the sensitivity of the technique. Similarly, calculations show, for the ideal stoichiometric interface, the presence of a fully spin-polarized charge only in the first STO layer at the interface, with a Ti magnetic moments 0.038 μ_B. This is consistent with what found in [22, 23] for Co and Ti magnetic overlayers, respectively, yet arguably too small to be univocally identified in x-rays experiments. Interestingly, the 2DEG charge is not produced by the usual Zener breakdown occurring between LAO valence band top states and STO band bottom, which is prevented by the strong depolarizing effect exerted by the metallic overlayer, but it is directly transferred from the LSMO overlayer to the interface. This aspect agrees with what found in [23] for a series of metallic overlayers on LAO/STO.

This work is organized as follows: in section 2 we describe the experimental and theoretical methods; in section 3 we describe the experimental results of in-plane transport and out-of-plane current-voltage

characteristics; in section 4 we present the experimental results of XMCD measurements; in section 5 we describe *ab-initio* calculations of the band structure in the LSMO/LAO/STO heterostructure; in section 6 we discuss consistency and significance of our findings on the basis of our combined experimental and theoretical inputs; finally in section 7 we summarize the conclusions of this work.

2. Experimental setting and theoretical methods

LSMO/LAO/STO heterostructures are deposited by pulsed laser deposition (PLD) on 5×5 mm^2 STO substrates, as described in [24, 25]. The same deposition conditions are adopted for both LAO and LSMO layers, i.e.: 5×10^{-2} mbar oxygen pressure, T = 740 °C substrate temperature, 1.5 J cm^{-2} laser spot fluence, 1 Hz repetition rate. The selected value of oxygen pressure is intermediate between those that are generally considered as optimal for LAO and LSMO pulsed laser deposition. The growth of high-quality oxide interfaces in such high-pressure regime, that makes the oxygen post-annealing procedure unnecessary, has been previously analyzed by some of the authors [25–27]. Morphology and roughness of each layer are monitored *in situ* by RHEED (Reflection High-Energy Electron Diffraction) diagnostics. Surface morphology was also inspected by *ex situ* atomic force microscopy (AFM).

In-plane and out-of-plane transport measurements were performed in a Physical Properties Measurements System (PPMS) by Quantum Design, with external instruments, in order to extend the measurable current-voltage range. Current-voltage characteristics were measured on the LSMO/LAO/STO heterostructure, before and after removing the LSMO layer in HCl [28]. In the latter case, an Au electrode was evaporated on the top of the LAO layer. Negative electrodes are in contact to the interface electron gas, while positive electrodes are attached either to LSMO or to Au.

In order to investigate spin polarization of the diffused electrons, XMCD measurements were performed across the Ti-L$_{2,3}$ edges at the X-Treme beamline of the Swiss Light Source, at low temperature (2 K) and high magnetic field (± 7 T) [29].

The XMCD signal, extracted as the difference between the absorption spectra for right- and left-circularly polarized light, is non-vanishing only in presence of a net magnetization. Since absorption energies for L$_{2,3}$ transitions are different for different chemical elements, we can discriminate between the magnetic signal of LSMO, evaluated from Mn-edge dichroism, and the one potentially related to diffused carriers in LAO/STO 2DES, evaluated from Ti-edge dichroism.

In order to enhance the sensitivity to the signal generated by the Ti atoms located at the LAO/STO interface, x-ray absorption spectra were recorded in total electron yield (TEY) detection mode by measuring the current drained through the LSMO layer.

In the examined samples, the thickness of the LSMO and LAO layers are 8 and 5 unit cells (u.c.), respectively. The thicknesses of the layers were chosen such that the total thickness of the heterostructure is not exceedingly high for detecting the x-ray absorption of Ti atoms by TEY. Additionally, the chosen LSMO thickness exceeds the critical value ~3 unit cells, below which the LSMO film is nonferromagnetic and nonmetallic [30, 31]. On the other hand, the chosen LAO thickness exceeds the critical value for the 2DEG formation in LAO/STO [32].

We mention that an early experiment was carried out by choosing different thickness parameters, namely LSMO(10 u.c.)/LAO(4 u.c.)/STO. Therein, the XMCD spectra indicated null spin polarization of Ti electrons and the expected spin polarization of Mn electrons. A subsequent wet etching of the LSMO overlayer and transport measurements of the LAO/STO remaining heterostructure indicated that no 2DEG was confined at the interface, explaining the absence of dichroic signal on Ti. Hence, the choice of 5 u.c. LAO thickness represents the minimum possible barrier thickness, which should maximize spin transfer.

The *ab-initio* VPSIC calculations [33, 34] were implemented in plane-wave plus ultrasoft pseudopotential (USPP) approach. At variance with ordinary local-spin density functional calculations (LSDA), the VPSIC allows the accurate determination of the electronic band structure for oxides and strong-correlated materials, including the fundamental band gap of insulating oxides and the band alignment in oxide-based heterostructures [35–38]. As an example, for the materials of interest in this work, the VPSIC-calculated band gap of LAO (5.4 eV) and STO (3.0 eV) are matching within less than 10% the experimental values, while differences of ~50% are typical for LSDA calculations. The VPSIC approach has been also applied to ferromagnetic manganites [39–41] with quite satisfying results. The heterostructure considered in our simulation is a bit smaller that the experimental one, but still adequate for our means. It includes 3 u.c. of LSMO, 4 u.c. of LAO, 11 u.c. of STO, and 3 u.c. of vacuum above LSMO. To avoid spurious fields due to periodic boundary conditions, the cell is further doubled along the [001] direction: the 11 u.c. long STO slab has a center of symmetry in the middle, and two LAO/LSMO/VACUUM heterostructures on both sides. By symmetry, these two sides are identical so that the only macroscopic field across the structure is in LAO, and genuinely due to the LAO polarity. The structure is fully relaxed along the *z* axis in a 1×1 symmetry, while the in-plane lattice
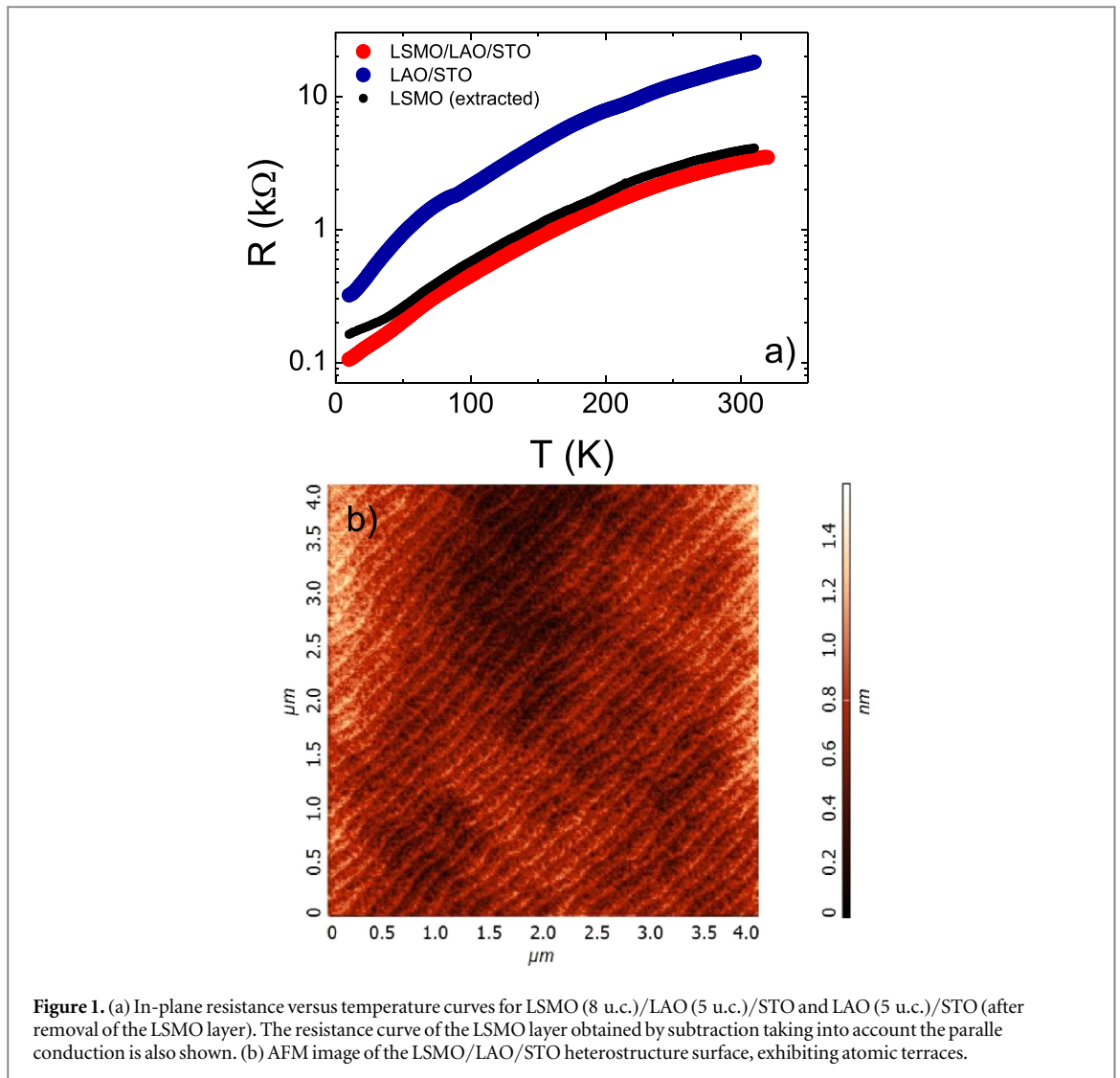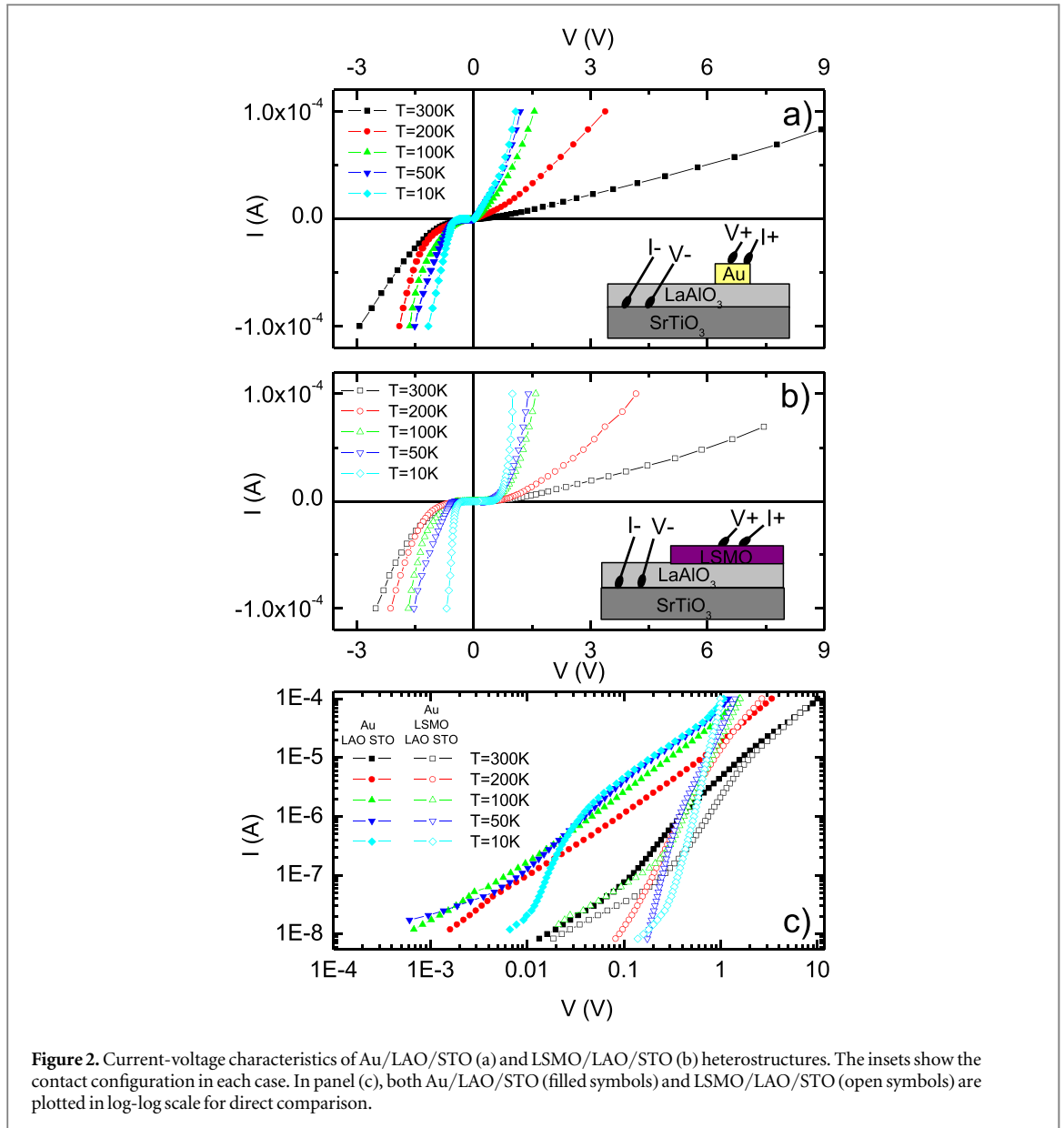
Figure 1. (a) In-plane resistance versus temperature curves for LSMO (8 u.c.)/LAO (5 u.c.)/STO and LAO (5 u.c.)/STO (after removal of the LSMO layer). The resistance curve of the LSMO layer obtained by subtraction taking into account the paralle conduction is also shown. (b) AFM image of the LSMO/LAO/STO heterostructure surface, exhibiting atomic terraces.

parameter is kept fixed at the theoretical STO bulk value $a = 3.905$ Å, which perfectly matches the experimental value. Doping in the manganite is treated through actual La-Sr atomic substitutions in the ratio of 1 Sr atom out of 3 La, so that a nominal hole doping of 33% with respect to $LaMnO_3$ is accounted for.

3. Results of in-plane transport and out-of-plane current-voltage characteristics

The optimized deposition conditions yield LSMO films with good magnetic behavior and good morphological and transport properties, despite the film thickness is only a few unit cells larger than the typical dead layer thickness [42]. In figure 1(a), the resistance R(T) curve measured in the LSMO/LAO/STO heterostructure is shown. Also shown in the same figure, the R(T) curve measured after removal of the LSMO layer by chemical etching indicates that the conducting properties of the underlying LAO/STO interface turns out perfectly consistent with those of simple LAO/STO interfaces. As the parallel layer transport in the LSMO/LAO/STO heterostructure is dominated by the less resistive LSMO layer, the R(T) curve reflects the behavior of LSMO itself, exhibiting metallic behavior up to 320 K. Indeed, from the two LSMO/LAO/STO and LAO/STO resistance curves, considering the parallel conduction, the LSMO resistance curve can be extracted by subtraction, and it exhibits metallic behavior in the whole measured temperature range. Hence, the metal-insulator transition that is always associated to the Curie temperature in manganite films must be at temperature above the measured range, demonstrating the high quality of the film. As for morphological properties, the heterostructure is atomically flat, with one unit cell terraces visible in AFM images (see figure 1(b)).

Moving to out-of-plane transport, figure 2 shows the current-voltage characteristics of the Au/LAO/STO (upper panel) and LSMO/LAO/STO (middle panel) heterostructures. In both cases, the curves are highly asymmetric and non linear. The Au/LAO/STO curves can be fitted by exponential Zener-type [43] or Fowler-Nordheim-type [44] mechanisms in the whole current range for positive bias and at high currents ($I > 10^{-6}$ A)

Figure 2. Current-voltage characteristics of Au/LAO/STO (a) and LSMO/LAO/STO (b) heterostructures. The insets show the contact configuration in each case. In panel (c), both Au/LAO/STO (filled symbols) and LSMO/LAO/STO (open symbols) are plotted in log-log scale for direct comparison.

for negative bias. The negative low-current regime can be described by direct tunneling behavior [45]. In agreement with the analysis of [46], there are two ranges dominated by different mechanisms for negative bias and a single mechanism valid in the whole range for positive bias. The additional LSMO layer does not change dramatically the shape of the current-voltage characteristics, as seen in figure 2(b). In the low-current regime, they exhibit a less regular behavior, which cannot be clearly described by any conventional mechanism. On the other hand, the high current regime is described by Zener-type or Fowler-Nordheim-type mechanisms for either polarity signs, as in the case of the Au/LAO/STO heterostructure. However, on a quantitative basis, it is apparent that the LSMO/LAO/STO heterostructure systematically exhibits lower currents than the Au/LAO/STO heterostructure at all temperatures, especially in the low-bias regime. This is seen in figure 2(c), where the curves of the two heterostructures are plotted in log-log scale for positive bias. This is also verified by comparing the values of fitting exponential coefficient C of the Zener mechanism ($I \propto V \cdot \exp(-C/V)$), which is systematically larger for the LSMO/LAO/STO heterostructure than for the Au/LAO/STO heterostructure. According to the Zener model, the exponential coefficient C is proportional to the product $m_z \cdot d \cdot \Phi_B^2$, where m_z is the effective mass along the tunneling direction across the barrier, d is the effective thickness of the barrier and Φ_B the energy barrier height. Hence, the barrier for tunneling can be associated to a larger ($m_z \cdot d \cdot \Phi_B^2$) product when an additional LSMO layer is stacked. Moreover, the additional LSMO layer makes the barrier more symmetric with respect to the bias sign.

The difference in the tunneling barrier between LSMO/LAO/STO and Au/LAO/STO may be due to (i) a different band alignment across the metallic contact/LAO interface, and (ii) the presence of a LSMO interfacial dead layer, which further enhances the barrier thickness provided by LAO. Eventually these two mechanisms
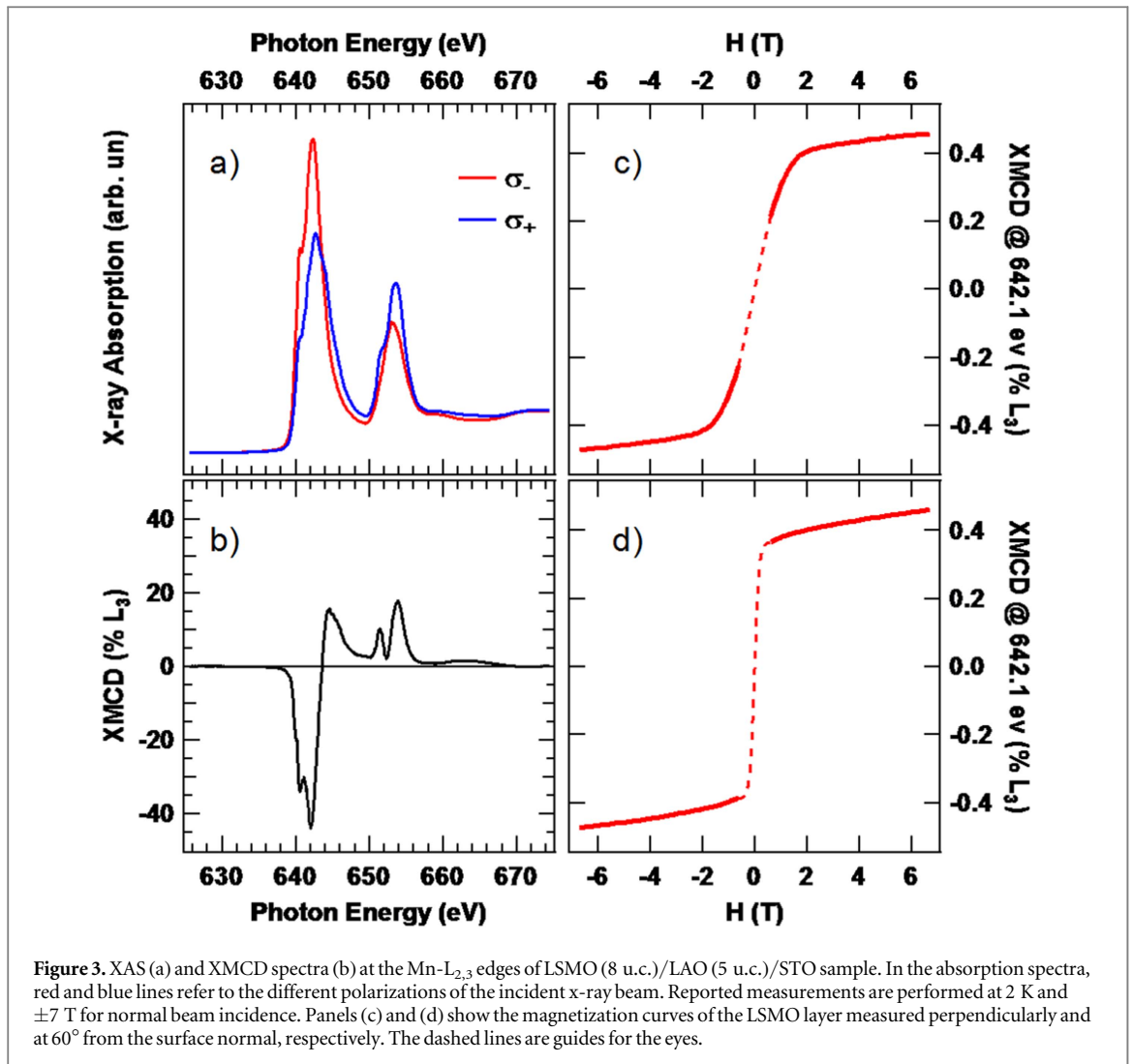
Figure 3. XAS (a) and XMCD spectra (b) at the Mn-$L_{2,3}$ edges of LSMO (8 u.c.)/LAO (5 u.c.)/STO sample. In the absorption spectra, red and blue lines refer to the different polarizations of the incident x-ray beam. Reported measurements are performed at 2 K and ± 7 T for normal beam incidence. Panels (c) and (d) show the magnetization curves of the LSMO layer measured perpendicularly and at 60° from the surface normal, respectively. The dashed lines are guides for the eyes.
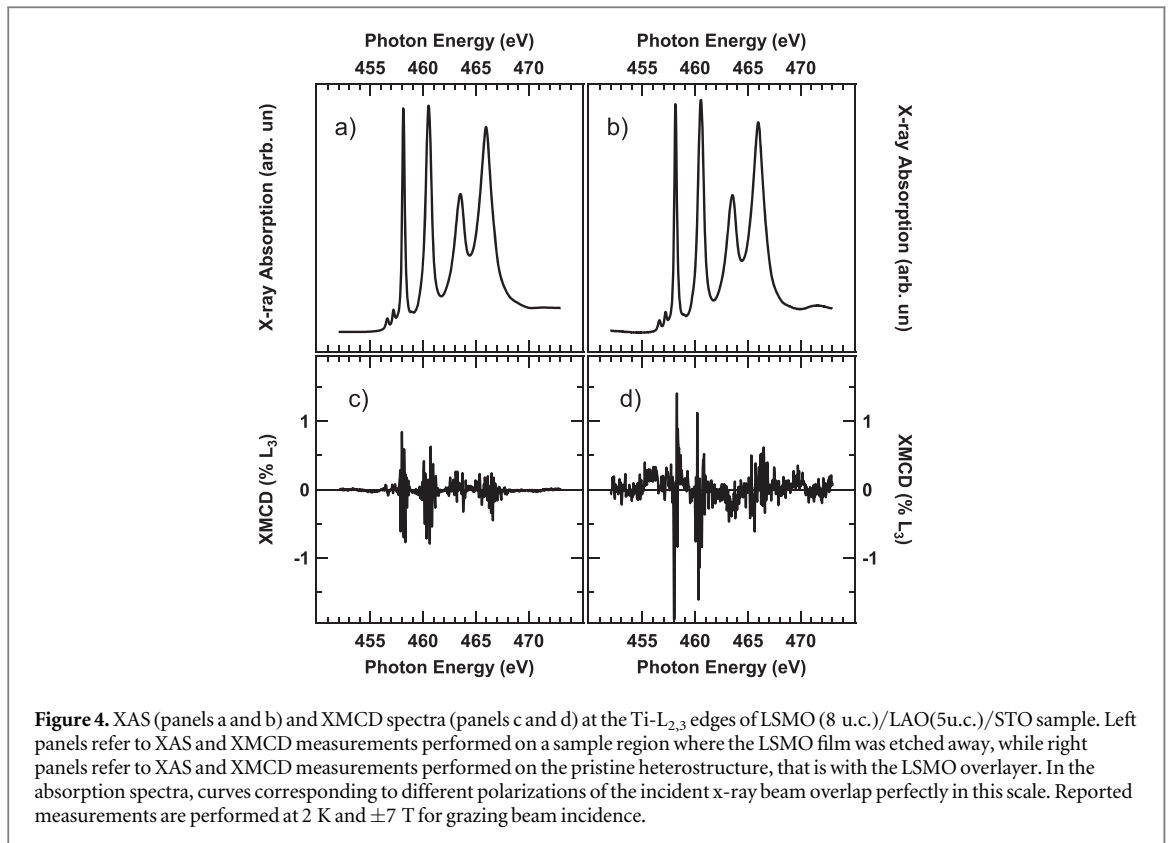
may combine, ultimately conveying a larger and more symmetric (with respect to voltage inversion) barrier for the heterostructure with the LSMO overlayer. Clearly, height and thickness of the barrier both work against the transfer of spin-polarized charge in the 2DEG, hindering the tunneling probability across the barrier. In section 5 we will analyze the energy barrier for the LSMO/LAO/STO heterostructure as derived by our *ab-initio* calculations.

4. Results of XAS and XMCD measurements

The magnetic properties of the LSMO layer were verified by XMCD measurement at the Mn-$L_{2,3}$ adsorption edges (figure 3, left panels) and by measuring the relative element-sensitive magnetization curve M(H) (figure 3, right panels).

The dichroic signal, shown in figure 3(b), is large, with a negative contribution in correspondence of about 642.1 eV and positive contribution around 653.9 eV, related to L_3 and L_2 absorption peaks clearly visible in the absorption spectra shown in figure 3(a). The XAS and XMCD spectra at the Mn-$L_{2,3}$ edges confirm the stoichiometric quality of our samples [47, 48]. The magnetization curves shown in the right panels of figure 3 were acquired while recording the intensity of the dichroic signal at 642.1 eV as a function of the external magnetic field, applied either perpendicularly (figure 1(c)) or at grazing angle (figure 1(d)) with respect to the film surface. The two magnetization curves confirm the FM character, with in-plane easy axis, of the LSMO film thus showing that ferromagnetism is preserved despite the fact that the LSMO thickness only slightly exceeds the expected dead layer thickness [30, 31].

To investigate the effect of the LSMO overlayer on the spin polarization of the 2DEG at the interface, we compared the XAS and XMCD spectra at the Ti-$L_{2,3}$ edges obtained from the LAO/STO interface buried underneath LSMO with the spectra obtained from a portion of the same sample where the LSMO layer was etched away. The corresponding XAS spectra, shown in panels a and b of figure 4, respectively, agree with those

Figure 4. XAS (panels a and b) and XMCD spectra (panels c and d) at the Ti-$L_{2,3}$ edges of LSMO (8 u.c.)/LAO(5u.c.)/STO sample. Left panels refer to XAS and XMCD measurements performed on a sample region where the LSMO film was etched away, while right panels refer to XAS and XMCD measurements performed on the pristine heterostructure, that is with the LSMO overlayer. In the absorption spectra, curves corresponding to different polarizations of the incident x-ray beam overlap perfectly in this scale. Reported measurements are performed at 2 K and ± 7 T for grazing beam incidence.
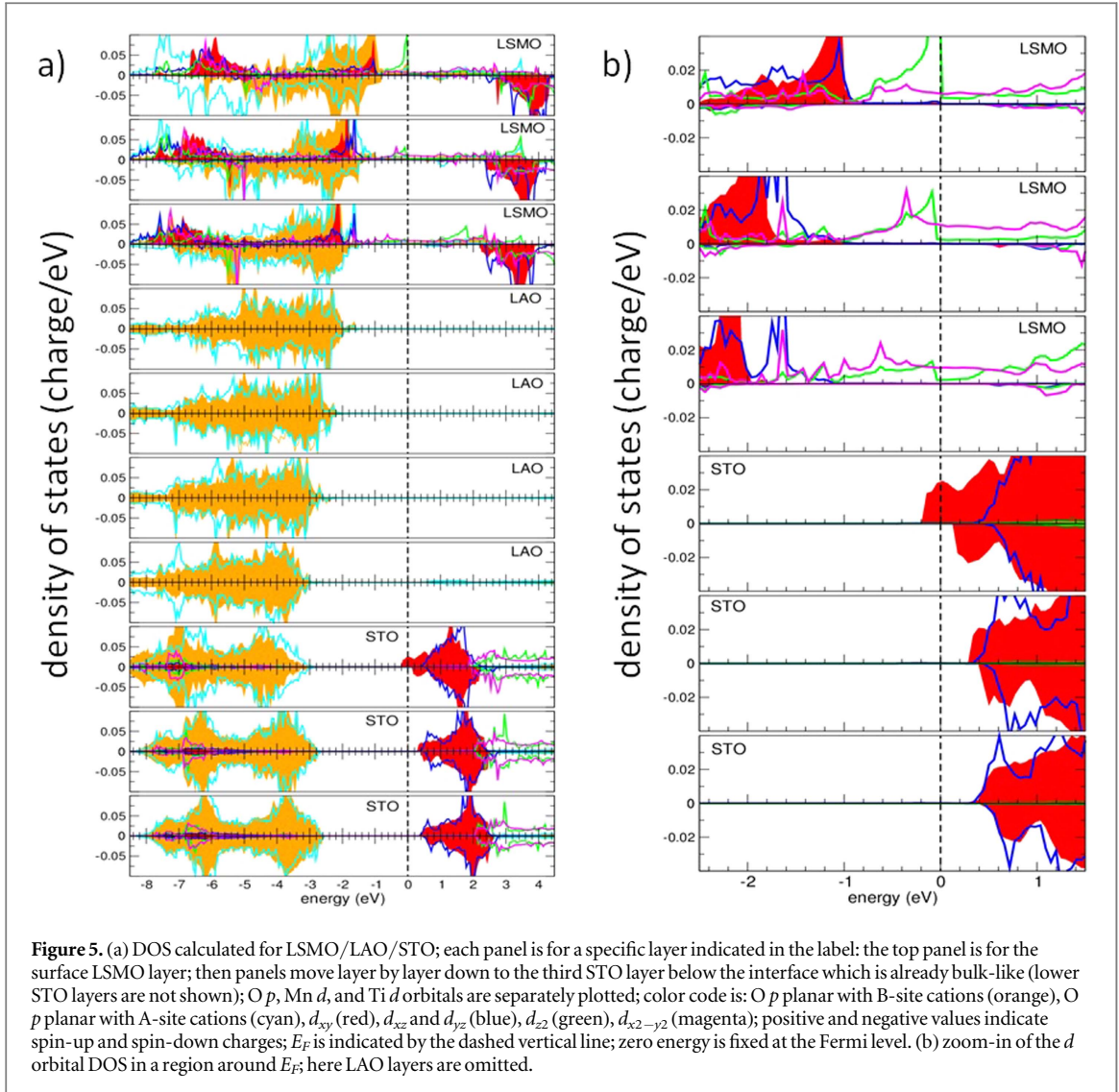
observed in bulk STO [49, 50] and LAO/STO [51] samples. This indicates the high quality of the samples and in particular the lack of oxygen vacancies at the LAO/STO interface [51].

In the lower panels of figure 4, we show XMCD measurements at the Ti-$L_{2,3}$ edges performed either after the etching of the LSMO film (panel c) or with the LSMO (panel d), carried out with grazing incident beam. It comes out that neither the XMCD measurements at the Ti-$L_{2,3}$ edges performed after the LSMO film etching, nor those performed with the LSMO film give any dichroic signal within our detection sensitivity (about 0.5% of the x-ray absorption signal). Measurements shown in figure 4 are related to grazing incident beam, however we find a null XMCD signal, within our detection sensitivity, also in other tested experimental conditions. Specifically, additional measurements were done by varying both the size of the area illuminated by the x-ray beam (in order to investigate the possible effects of the different energy and drained-current density) and the orientation of the sample with respect to the external magnetic field and the x-ray beam direction (in order to sample different components of the induced magnetization).

Considering extrinsic effect that inevitably affect LAO/STO samples (discussed in the following), the lack of any significant XMCD signal in our LAO/STO sample without LSMO on top, indicating absence of a sizeable net magnetization in the bare 2DEG, is compatible with the case of the LAO/STO samples of [51], where only a tiny signal was detected. Here we show that the additional presence of the magnetic LSMO overlayer does not induce any further sizeable spin polarization in the 2D electron gas.
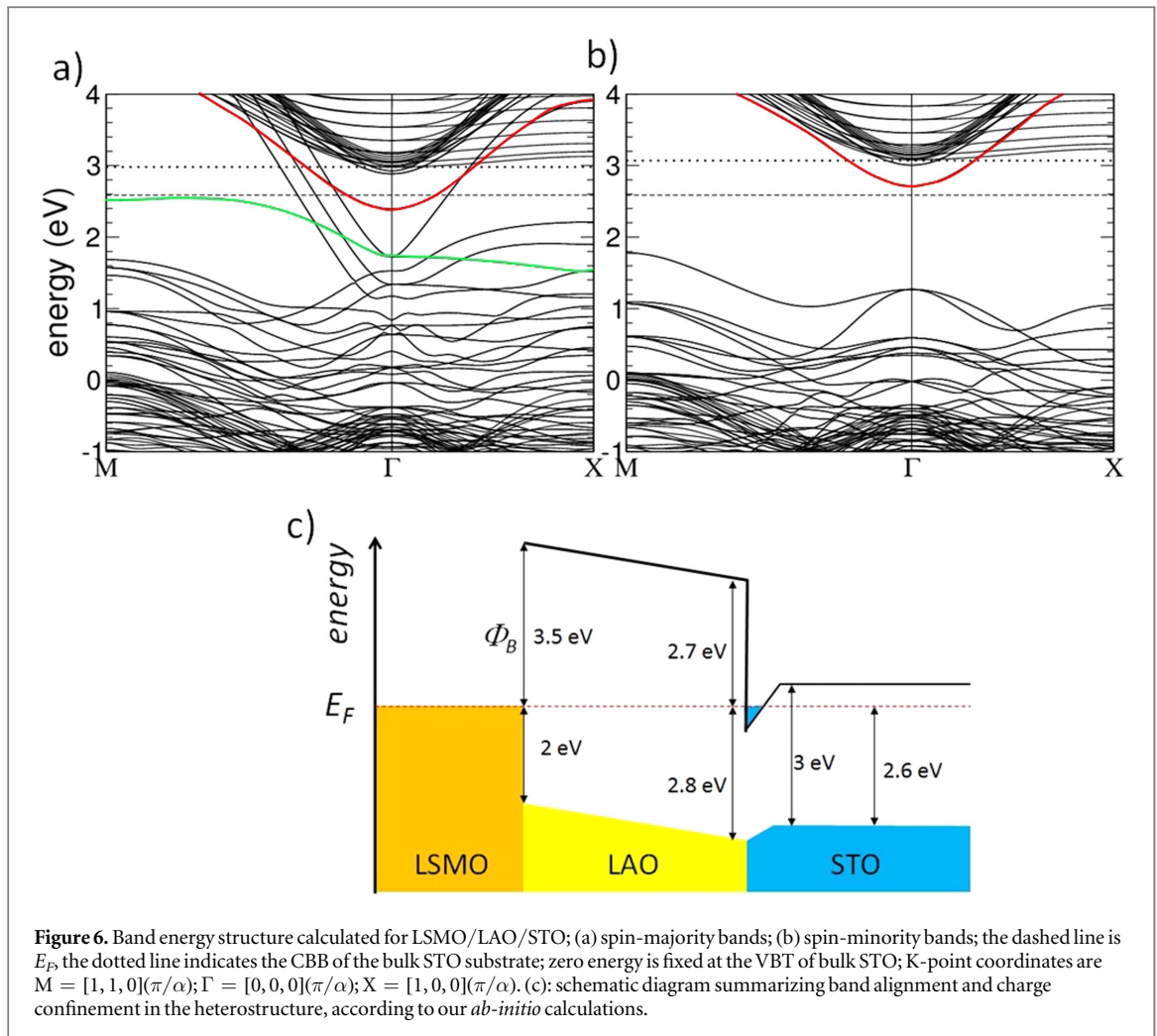
5. *Ab-initio* calculations

The calculated density of states (DOS) of the LSMO/LAO/STO heterostructure is plotted in figure 5, disentangled in separate layers, each of them resolved in different orbital contributions. Moving through the panels from top (LSMO surface) to bottom (STO substrate), the potential line-up along the confinement direction (z = [001]) can be easily understood. We can see that the LSMO layers are half-metallic, i.e. fully spin-polarized around the Fermi energy. The presence of LSMO drastically modifies the band diagram of LAO/STO, by providing carriers at the Fermi surface of LSMO which lies well above the LAO valence band. Such carriers will screen the polar catastrophe by anticipating the electronic reconstruction normally taking place, in uncapped interfaces, from the LAO valence band top (VBT) to the STO conduction band bottom (CBB). This reduces in turn the LAO potential build-up, from the ~3 eV normally required to induce the Zener breakdown to less than 1 eV. Nevertheless, we see that some conduction charge at the LAO/STO interface is actually present, as a result of a spontaneous charge transfer from LSMO to STO. This charge is visibly spin-polarized, and strictly confined in the first STO layer at the LAO/STO interface.

Figure 5. (a) DOS calculated for LSMO/LAO/STO; each panel is for a specific layer indicated in the label: the top panel is for the surface LSMO layer; then panels move layer by layer down to the third STO layer below the interface which is already bulk-like (lower STO layers are not shown); O *p*, Mn *d*, and Ti *d* orbitals are separately plotted; color code is: O *p* planar with B-site cations (orange), O *p* planar with A-site cations (cyan), d_{xy} (red), d_{xz} and d_{yz} (blue), d_{z2} (green), d_{x2-y2} (magenta); positive and negative values indicate spin-up and spin-down charges; E_F is indicated by the dashed vertical line; zero energy is fixed at the Fermi level. (b) zoom-in of the *d* orbital DOS in a region around E_F; here LAO layers are omitted.

Let us come to analyze the properties of the well more in detail, starting with the LSMO surface layer. At the surface a substantial spin-polarization is visible, with a total Mn magnetic moment of 3.76 μ_B, consistent with a nominal Mn^{3+} ionic configuration; Mn shows a fully spin-polarized $3d$ t_{2g} shell (red-shaded line for d_{xy} and blue line for the d_{xz}/d_{yz} doublet, respectively) which accounts for 2.73 μ_B out of the total magnetic moment, while an additional contribution comes from e_g's (0.60 μ_B from d_{z2} and 0.43 μ_B from d_{x2-y2}). The t_{2g} spin-splitting at the surface is around 10 eV, as customary for $3d$ shells in cubic symmetry; the t_{2g} majority DOS extends up to about 1 eV below E_F, and the t_{2g} minority DOS starts about 2.5 eV above E_F. The region from 1 eV below E_F up to 2.5 eV above E_F is entirely filled by fully polarized e_g states, hybridized with in-plane O *p* states.

In the enlarged DOS of figure 5(b) we see that just below E_F there is a high d_{z2} peak which derives from a localized state at the surface, while the d_{x2-y2} DOS spreads smoothly across the Fermi energy region. The other LSMO layers below the surface are not much different: the two e_g orbitals become progressively close to each other as we get farther from the surface, and the Mn magnetic moments are just a bit smaller than for the surface layer (3.59 μ_B and 3.60 μ_B for second and third layer, respectively). Analysing the DOS of STO layers we can see two remarkable aspects: the CBB of d_{xy} character in the first STO layer extends slightly (~0.2 eV) below E_F, while already at the second STO layer the CBB remains well above E_F; in other words, although some charge is spontaneously transferred from LSMO to STO, it remains extremely confined at the interface. According to our integrated DOS, this charge amounts to $n_s = 2.5 \times 10^{13}$ cm^{-2}, thus it is comparable to that observed in LAO/STO and slightly smaller than that ($n_s \sim 5 \times 10^{13}$ cm^{-2}) calculated in LAO/STO for a 4 u.c. LAO layer. Furthermore, this charge is fully spin-polarized, and corresponds to a Ti magnetic moment of 0.038 μ_B. In figure 5(b) we see that some spin-splitting is visible up to the second STO layer from the interface, while from the third STO layer the DOS recovers a spin-degenerate aspect. Interestingly, the spin polarization is visibly larger for d_{xy} than for the d_{xz}/d_{yz} doublet. Overall, our calculated DOS in figure 5 is substantially similar to the DOS

Figure 6. Band energy structure calculated for LSMO/LAO/STO; (a) spin-majority bands; (b) spin-minority bands; the dashed line is E_F, the dotted line indicates the CBB of the bulk STO substrate; zero energy is fixed at the VBT of bulk STO; K-point coordinates are $M = [1, 1, 0](\pi/\alpha); \Gamma = [0, 0, 0](\pi/\alpha); X = [1, 0, 0](\pi/\alpha)$. (c): schematic diagram summarizing band alignment and charge confinement in the heterostructure, according to our *ab-initio* calculations.

calculated in [22] for the Co monolayer, and in [23] for the Ti monolayer; in all these cases the transferred moment amounts to a few hundredths of a μ_B per atom.

Some aspects of the systems can be better appreciated from the band diagram reported in figure 6. Here the half-metallic character is immediately apparent from the band gap opened in the minority channel. Zero energy is fixed at the valence band top (VBT) of the innermost STO layer, occurring at M point. Above that, there is a mixture of O p and Mn t_{2g} states from LAO and LSMO. In particular, we can see a band in the majority manifold (green-coloured in figure 6(a)) running just slightly below E_F: this is the d_{z2} surface state described in the DOS, observed in the top panel of figures 5(a) and (b). Then we have three bands crossing E_F, which derive from Mn e_g's—O p hybridized states. The highest-energy band crossing E_F (red-coloured in figure 6) derives from the spin-polarized d_{xy} orbital sited on the first Ti layer at the interface. Its bottom in the majority channel lies 0.19 eV below E_F at Γ point, and it is split from the minority counterpart by 0.32 eV. The spin splitting reduces to 0.12 eV for the unoccupied d_{xy} band sited on the second Ti layer from the interface, while it is only 0.09 eV for the unoccupied d_{xz}/d_{yz} doublet. In figure 6(c) we draw a schematic diagram summarizing the band alignment across the heterostructure as described by our calculations. A crucial aspect concerns the position of E_F, which lies ~0.4 eV below the CBB of the STO substrate, and ~3.5 eV below the LAO CBB in correspondence of the LSMO/ LAO interface. The latter energy gives the tunnelling barrier Φ_B for perpendicular transport between LSMO and the 2DEG, and then it governs the I-V behaviour described in the previous section. Such a large barrier is also a key aspect in the reduction of spin-polarization transmission from LSMO to STO in equilibrium conditions, since the spin-polarized Mn 3d wavefunctions, while tunnelling across the LAO barrier, decay exponentially with the square root of Φ_B.

6. Discussion

The picture emerging from our experimental/computational study draws a rather complex landscape for the LSMO-capped LAO/STO heterostructure. *Ab-initio* calculations show that, on one hand, the LSMO overlayer

compensates the polar catastrophe and prevents the occurrence of Zener breakdown; on the other, it directly instils a charge density $n_s = 2.5 \times 10^{13}\,\mathrm{cm}^{-2}$ of d_{xy} character in the STO conduction bands. This charge is spin-polarized (with magnetic moment per Ti atom ∼0.038 μ_B) and confined in just a single STO layer at the interface. Calculations also reveal the presence of empty, spin-split conduction bands of d_{xy} character in the second STO layers below the interface, while from the third STO layer and beyond the conduction bands are substantially spin degenerate. Thus, even in case of a field-effect modulation widening the 2DEG thickness, we do not expect any relevant strengthening of the magnetism at the interface.

In this scenario, it is rather challenging to reveal such a small and spatially confined magnetization resulting from the calculations. Indeed, being confined to the first interfacial layer, the XCMD signal due to the small magnetization is further attenuated by the total sampling depth of the TEY measurement. In fact, considering an exponential decay of the TEY signal as a function of the depth from surface and assuming a reasonable decay length of 4 nm, we obtain that the first STO layer (the only one which carries a magnetic moment) contributes for about 10% of the total Ti XAS signal. This approximate evaluation shows with great immediacy the difficulty of revealing the calculated magnetic moment by XMCD measurements. Yet, these considerations leave an open possibility that a spin-polarized 2DEG, albeit small and difficult to reveal, may actually exists, and be exploited in spin-transport applications. On the other hand, calculations assume a pristine heterostructure and do not include structural disorder, additional extrinsic doping, and the ubiquitous dead-layer at the LSMO interface, all aspects which most likely hamper or further reduce the 'ideal' spin polarization transfer in real samples. Indeed, the presence or the lack of a spin-resolved charge could be then crucially related to the very specific characteristics of the considered sample. According to this interpretation, spin-polarized transport in LAO/STO would be a substantially fragile occurrence, thus accounting for the apparent contrast in the existing literature between cases of substantial [18–20] or marginal [22, 23] presence of spin-polarization at the LAO/STO interface as transferred from FM electrodes.

7. Conclusions

We investigated the presence of a spin polarized 2DEG in the LSMO/LAO/STO heterostructure, using a combined experimental and theoretical approach. XMCD data give no evidence of transfer of spin polarized carriers from the ferromagnetic LSMO layer into the 2DEG. In addition, out-of-plane current-voltage transport measurements indicate that the tunneling barrier in LSMO/LAO/STO is larger and more symmetric, with respect to the bias sign, than in Au/LAO/STO, likely as a consequence of the presence of a dead layer at the LSMO interface. Our *ab-initio* calculations of structural and electronic properties for the stoichiometric LSMO/LAO/STO heterostructure predict that some spin-resolved mobile charge in STO does exist, but it generates tiny magnetization (∼0.038 μ_B per Ti atom) and is extremely confined in space (i.e. restricted to a single STO layer adjacent to LAO). The small spin-transfer capability of LSMO across LAO is ultimately motivated by the large LSMO/LAO energy barrier for tunneling (equal to 3.5 eV according to our calculations). This small and confined magnetization is compatible in magnitude with the nul result of XMCD measurements, considering that such tiny effect may be plausibly washed out by extrinsic aspects, such as structural disorder, doping and presence of a LSMO dead-layer, which explains the spread of results found in literature [18–20, 22]. Overall, our results indicate that spin transfer from LSMO to the 2DEG is actually possible for the pristine heterostructure, although difficult to achieve in practice.

Acknowledgments

ORCID iDs

I Pallecchi ⓘ https://orcid.org/0000-0001-6819-6124
G Vinai ⓘ https://orcid.org/0000-0003-4882-663X

References

[1] Ohtomo A and Hwang H Y 2004 A high-mobility electron gas at the LaAlO₃/SrTiO₃ heterointerface *Nature* **427** 423
[2] Zubko. P, Gariglio S, Gabay M, Ghosez P and Triscone J-M 2011 Interface physics in complex oxide heterostructures *Annu. Rev. Mater. Res.* **2** 141–65

[3] Sulpizio J A, Ilani S, Irvin P and Levy J 2014 Nanoscale phenomena in oxide heterostructures *Annual Review of Materials Research* **44** 117–49

[4] Caviglia A D, Gabay M, Gariglio S, Reyren N, Cancellieri C and Triscone J-M 2010 Tunable rashba spin—orbit interaction at oxide interfaces *Phys. Rev. Lett.* **104** 126803

[5] Jin M-J *et al* 2017 *Nano Lett.* **17** 36–43

[6] Pavlenko N, Kopp T, Tsymbal E Y, Sawatzky G A and Mannhart J 2012 Magnetic and superconducting phases at the LaAlO$_3$/SrTiO$_3$ interface: the role of interfacial Ti 3d electrons *Phys. Rev.* B **85** 020407(R)

[7] Fix T, Schoofs F, MacManus-Driscoll J L and Blamire M G 2010 Influence of doping at the nanoscale at LaAlO$_3$/SrTiO$_3$ interfaces *Appl. Phys. Lett.* **97** 072110

[8] Rastogi A, Pulikkotil J J, Hossain Z, Kumar D and Budhani R C 2014 δ-doped LaAlO$_3$-SrTiO$_3$ interface: electrical transport and characterization of the interface potential *Europhys. Lett.* **106** 57002

[9] Di Capua R *et al* 2014 Transport properties of a quasi-two-dimensional electron system formed in LaAlO$_3$/EuTiO$_3$/SrTiO$_3$ heterostructures *Phys. Rev.* B **89** 224413

[10] Stornaiuolo D *et al* 2016 Tunable spin polarization and superconductivity in engineered oxide interfaces *Nat. Mater.* **15** 278

[11] Zhang H R *et al* 2017 *Phys. Rev.* B **96** 195167

[12] Liu H-J *et al* 2016 *Adv. Mater.* **28** 9142–51

[13] Chauleau J-Y, Boselli M, Gariglio S, Weil R, de Loubens G, Triscone J-M and Viret M 2016 *Europhys. Lett.* **116** 17006

[14] Song Q, Zhang H, Su T, Yuan W, Chen Y, Xing W, Shi J, Sun J and Han W 2017 *Sci. Adv.* **3** e1602312

[15] Wang Y, Ramaswamy R, Motapothula M, Narayanapillai K, Zhu D, Yu J, Venkatesan T and Yang H 2017 Room-temperature giant charge-to-spin conversion at the SrTiO3-LaAlO3 oxide interface *Nano. Lett.* **17** 7659–64

[16] Lü W M *et al* 2016 Long-range magnetic coupling across a polar insulating layer *Nat. Commun.* **7** 11015

[17] Epstein R J, Malajovich I, Kawakami R K, Chye Y, Hanson M, Petroff P M, Gossard A C and Awschalom D D 2002 Spontaneous spin coherence in n-GaAs produced by ferromagnetic proximity polarization *Phys. Rev.* B **65** 121202(R)

[18] Reyren N, Bibes M, Lesne E, George J-M, Deranlot C, Collin S, Barthélémy A and Jaffrès H 2012 Gate-controlled spin injection at LaAlO$_3$/SrTiO$_3$ interfaces *Phys. Rev. Lett.* **108** 186802

[19] Ngo T D N *et al* 2015 Polarity-tunable magnetic tunnel junctions based on ferromagnetism at oxide heterointerfaces *Nat. Commun.* **6** 8035

[20] Ohshima R *et al* 2017 Strong evidence for d-electron spin transport at room temperature at a LaAlO$_3$/SrTiO$_3$ interface *Nat. Mater.* **16** 609–14

[21] Sahin C, Vignale G and Flatté M E 2014 Derivation of effective spin—orbit hamiltonians and spin lifetimes with application to SrTiO$_3$ heterostructures *Phys. Rev.* B **89** 155402

[22] Lesne E *et al* 2014 Suppression of the critical thickness threshold for conductivity at the LaAlO$_3$/SrTiO$_3$ interface *Nat. Commun.* **5** 4291

[23] Arras R, Ruiz V G, Pickett W E and Pentcheva R 2012 Tuning the two-dimensional electron gas at the LaAlO$_3$/SrTiO$_3$(001) interface by metallic contacts *Phys. Rev.* B **85** 125404

[24] Parlato L *et al* 2013 Time-resolved optical response of all-oxide YBa$_2$Cu$_3$O$_7$/La$_{0.7}$Sr$_{0.3}$MnO$_3$ proximitized bilayers *Phys. Rev.* B **87** 134514

[25] Aruta C, Amoruso S, Bruzzese R, Wang X, Maccariello D, Miletto Granozio F and Scotti di Uccio U 2010 Pulsed laser deposition of SrTiO$_3$/LaGaO$_3$ and SrTiO$_3$/LaAlO$_3$: plasma plume effects *Appl. Phys. Lett.* **97** 252105

[26] Di Gennaro E *et al* 2013 Persistent photoconductivity in 2D electron gases at different oxide interfaces *Adv. Opt. Mat.* **1** 834

[27] Aruta C *et al* 2012 Critical influence of target-to-substrate distance on conductive properties of LaGaO$_3$/SrTiO$_3$ interfaces deposited at 10^{-1} mbar oxygen pressure *Appl. Phys. Lett.* **101** 031602

[28] Telesio F, Pellegrino L, Pallecchi I, Marré D, Esposito E, di Gennaro E, Khare Amit and Miletto Granozio F 2016 Nano-patterning process based on epitaxial masking for the fabrication of electronic and spintronic devices made of La$_{0.67}$Sr$_{0.33}$MnO$_3$/LaAlO$_3$/SrTiO$_3$ heterostructures with *in situ* interfaces *J. Vac. Sci. Technol.* B **34** 011208

[29] Piamonteze C *et al* 2102 X-treme beamline at SLS: x-ray magnetic circular and linear dichroism at high field and low temperature *J. Shyncrotron. Rad.* **19** 661–74

[30] Stadler S, Idzerda Y U, Chen Z, Ogale S B and Venkatesan T 1999 The magnetism of a buried La$_{0.7}$Sr$_{0.3}$MnO$_3$ interface *Appl. Phys. Lett.* **75** 3384

[31] Huijben M, Martin L W, ChuM Y-H, Holcomb B, Yu P, Rijnders G, Blank D H A and Ramesh R 2008 Critical thickness and orbital ordering in ultrathin La$_{0.7}$Sr$_{0.3}$MnO$_3$ films *Phys. Rev.* B **78** 094413

[32] Thiel S, Hammerl G, Schmehl A, Schneider C W and Mannhart J 2006 Tunable quasi-two-dimensional electron gases in oxide heterostructures *Science* **313** 1942

[33] Filippetti A, Pemmaraju C D, Puggioni D, Delugas P, Fiorentini V and Sanvito S 2011 Introducing a variational pseudo-self-interaction correction approach for solids and molecules *Phys. Rev.* B **84** 195127

[34] Archer T *et al* 2011 Exchange interactions and magnetic phases of transition metal oxides: benchmarking advanced *ab initio* methods *Phys. Rev.* B **84** 115114

[35] Puggioni D, Filippetti A and Fiorentini V 2012 Ordering and multiple phase transitions in ultra-thin nickelate superlattices *Phys. Rev.* B **86** 195132

[36] Filippetti A, Delugas P, Verstraete M J, Pallecchi I, Gadaleta A, Marré D, Li D F, Gariglio S and Fiorentini V 2012 Thermopower in oxide heterostructures: the importance of being multiple-band conductors *Phys. Rev.* B **86** 195301

[37] Delugas P, Filippetti A, Verstraete M, Pallecchi I, Marrè D and Fiorentini V 2013 Doping-induced dimensional crossover and thermopower burst in Nb-doped SrTiO$_3$ superlattices *Phys. Rev.* B **88** 045310

[38] Delugas P, Filippetti A, Gadaleta A, Pallecchi I, Marré D and Fiorentini V 2013 Large band offset as driving force of 2-dimensional electron confinement: the case of SrTiO$_3$/SrZrO$_3$ interface *Phys. Rev.* B **88** 115304

[39] Filippetti A and Fiorentini V 2006 Double-exchange driven metal-insulator transition in Mn-doped CuO *Phys. Rev.* B *(Rapid Comm.)* **74** 220401

[40] Colizzi G, Filippetti A, Cossu F and Fiorentini V 2008 Interplay of strain and magnetism of La$_2$/3Sr1/3MnO$_3$ from first principles *Phys. Rev.* B **78** 235122

[41] Hao X F, Stroppa A, Picozzi S, Filippetti A and Franchini C 2012 Exceptionally large room-temperature ferroelectric polarization in the novel PbNiO$_3$ *Phys. Rev.* B **86** 014116

[42] Huijben M, Martin L W, Chu Y-H, Holcomb M B, Yu P, Rijnders G, Blank D H A and Ramesh R 2008 Critical thickness and orbital ordering in ultrathin La$_{0.7}$Sr$_{0.3}$MnO$_3$ films *Phys. Rev.* B **78** 094413

[43] Zener C 1934 A theory of electrical breakdown of solid dielectrics *Proc. R. Soc.* A **145** 523–9

[44] Fowler R H and Nordheim L 1928 Electron emission in intense electric fields *Proc. R. Soc.* A **119** 173–81

[45] Simmons J G 1963 Low-voltage current-voltage relationship of tunnel junctions *J. Appl. Phys.* **34** 238–9

[46] Singh-Bhalla G, Bell C, Ravichandran J, Siemons W, Hikita Y, Salahuddin S, Hebard A F, Hwang H Y and Ramesh R 2011 Built-in and induced polarization across $LaAlO_3/SrTiO_3$ heterojunctions *Nat. Phys.* **7** 80

[47] Abbate M *et al* 1992 Controlled-valence properties of $La_{1-x}Sr_xFeO_3$ and $La_{1-x}Sr_xMnO_3$ studied by soft-x-ray absorption spectroscopy *Phys. Rev.* B **46** 4511

[48] de Jong M P, Bergenti I, Dediu V A, Fahlman M, Marsi M and Taliani C 2005 Evidence for Mn^{2+} ions at surfaces of $La_{0.7}Sr_{0.3}MnO_3$ thin films *Phys. Rev.* B **71** 014434

[49] van der Laan G 1990 Polaronic satellites in x-ray-absorption spectra *Phys. Rev.* B **41** 12366(R)

[50] de Groot F M F 1994 X-ray absorption and dichroism of transition metals and their compounds *J. Electron Spectrosc. Relat. Phenom.* **67** 529

[51] Salluzzo M *et al* 2013 Origin of interface magnetism in $BiMnO_3/SrTiO_3$ and $LaAlO_3/SrTiO_3$ heterostructures *Phys. Rev. Lett.* **111** 087204